

DUET: Cross-modal Semantic Grounding for Contrastive Zero-shot Learning

Zhuo Chen, Yufeng Huang, Jiaoyan Chen, Yuxia Geng, Wen Zhang, Yin Fang, Jeff Z. Pan, Wenting Song, Huajun Chen

Abstract

Zero-shot learning (ZSL) aims to predict unseen classes whose samples have never appeared during training. One of the most effective and widely used semantic information for zero-shot image classification are attributes which are annotations for class-level visual characteristics. However, the current methods often fail to discriminate those subtle visual distinctions between images due to not only the shortage of fine-grained annotations, but also the attribute imbalance and co-occurrence. In this paper, we present a transformer-based end-to-end ZSL method named DUET, which integrates latent semantic knowledge from the pre-trained language models (PLMs) via a self-supervised multi-modal learning paradigm. Specifically, we (1) developed a cross-modal semantic grounding network to investigate the model’s capability of disentangling semantic attributes from the images; (2) applied an attribute-level contrastive learning strategy to further enhance the model’s discrimination on fine-grained visual characteristics against the attribute co-occurrence and imbalance; (3) proposed a multi-task learning policy for considering multi-model objectives. With extensive experiments on three standard ZSL benchmarks and a knowledge graph equipped ZSL benchmark, we find that DUET can often achieve state-of-the-art performance, its components are effective and its predictions are interpretable.

1 Introduction

Zero-shot learning (ZSL) aims to mimic human’s inference ability to learn novel concepts based on prior experience without seeing them beforehand. Early embedding-based ZSL methods (Frome et al. 2013) project the input into a common vector space where the unseen class prediction can be implemented by searching the nearest class. Generative ZSL methods (Chen et al. 2021g,d) create synthetic data via the semantic information of unseen classes, which strategically transforms ZSL into a standard supervised learning problem, and has less bias toward seen or unseen classes.

Attributes, which are annotations for image visual characteristics, are one of the most popular semantic information for zero-shot image classification. However, the attributes in real world are always not annotated to image regions but to a whole class. Recently, some attention-based ZSL

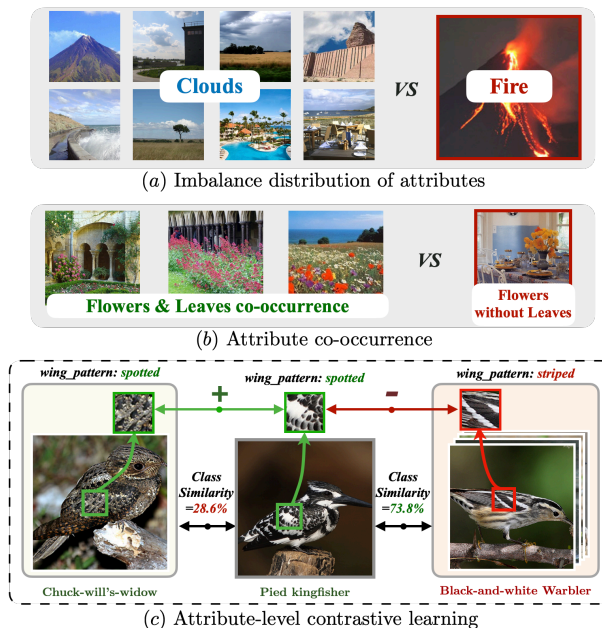


Figure 1: (a) Attribute imbalance. (b) Attribute co-occurrence. (c) Our attribute-level contrastive learning strategy which chooses those distinctive classes as positive references when they are associated with one common attribute (e.g., “spotted”) and those similar classes as negative references when they have mutually exclusive attributes (e.g., “striped”) toward the same aspect (e.g., “wing_pattern”).

methods (Chen et al. 2022b,a) emerge to distinguish the discriminative regions in image classification under the guidance of attentive attribute information. But as the discussion in (Zhao et al. 2019; Wang et al. 2021a), these systems all suffer from the *imbalanced attribute distribution* (i.e., some attributes are highly frequent while some are rare), as well as the *attribute co-occurrence* which impacts attributes’ discrimination capability. For example, in a zero-shot scene classification dataset SUN (Patterson and Hays 2012), the attributes “trees” and “clouds” are associated with 301 and 318 classes, respectively; but “railroad” and “fire” only appear in 15 and 10 classes. Besides, “flowers” appears with “leaves” 39 times, but “flowers” alone only appears 10 times; “grass” appears with “trees” 239 times, but

”grass” alone only appears 38 times (see Appendix for detailed statistics). Those distribution bias may influence the model’s judgment on those unseen classes which contain *rare attributes or new attribute combinations*.

To address these problems, in this paper, we propose a novel end-to-end ZSL framework named **DUET** (Cross-modal Semantic GroUding for ContrastivE Zero-shot Learning). Unlike previous ZSL methods in Figure 2(a) that emphasize utilizing more external class knowledge, augmenting data, or developing better vision encoders, we focus on transferring knowledge from PLMs to vision transformer encoder in a self-supervised manner, as shown in Figure 2(b), which gives the model the ability for *fine-grained semantic grounding* (i.e., the ability for locating relevant visual characteristics in an image given a textual attribute).

Specifically, we utilize a prompt-based Feature-to-Sequence Transformation (FST) proxy to transform different types of attributes into a textual sequence, which makes our model compatible to multiple ZSL tasks with different semantic information. A Cross-modal Semantic Grounding (CSG) network is developed to leverage the semantics in a PLM via a multi-task learning procedure, where we employ two switchable learning objectives: basic ZSL classification and cross-modal mask reconstruction (CMR). Moreover, we propose an attribute-level contrastive learning (ACL) mechanism as shown in Figure 1(c), where distinctive classes are selected as positive references when they are associated with one common attribute (e.g., “spotted”) and those similar classes as negative references when they have mutually exclusive attributes (e.g., “striped”) toward the same aspect (e.g., “wing_pattern”) of the image. This mechanism enables the model to distinguish subtle attribute differences between closed images, and find out the overlapped features between different images. The contributions can be summarized as:

- To the best of our knowledge, DUET is the first to investigate PLMs for zero-shot image classification. It includes a novel end-to-end multi-modal learning paradigm.
- A cross-modal semantic grounding network is developed for effective knowledge transfer from the PLM to the vision transformer encoder. An attribute-level contrastive learning mechanism is proposed to address the attribute imbalance and co-occurrence issues, which further enhances the model’s ability for distinguishing fine-grained vision characteristics in both seen/unseen images.
- Extensive experiments have been done on three standard ZSL benchmarks equipped with attributes and one ZSL benchmark equipped with a knowledge graph (KG). The results have verified the state-of-the-art performance of DUET as well as the effectiveness of its components and its interpretation capability. Our code will be available soon.

2 Related Work

2.1 Zero-shot Image Classification

The core idea of zero-shot image classification is to transfer semantic knowledge from seen classes to unseen classes based on their semantic information (Chen et al. 2021a,b),

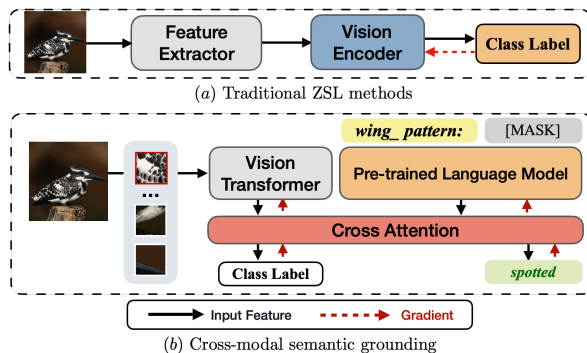


Figure 2: (a) The paradigm of previous ZSL methods. (b) The paradigm of our method DUET which exploits the semantics of PLMs to augment the transformer-based vision encoder via reconstructing masked attributes (e.g., “spotted”) with a cross-model attention mechanism.

e.g., a new bird could be identified according to its common color and shape as other birds that have training images.

Embedding-based ZSL methods (Frome et al. 2013) intend to build mapping functions toward the images and/or the classes, and whether a class is the label of a sample can be determined by matching their vectors in the same space using similarity metrics. However, their capabilities in transferring knowledge are restricted by semantic loss, while the lack of visual samples for the unseen classes causes the bias problem. To mitigate this issue, the **Generative** ZSL methods (2021d; 2021c; 2021a) are introduced to use various generative models (e.g., VAEs (2021f; 2021d) and GANs (2020a; 2021)) for creating synthetic data based on semantic features (e.g., simple attribute values (2021), knowledge graphs (2021a) or textual descriptions (2021)). This data augmentation strategy can compensate for the shortage of unseen classes and convert ZSL into a supervised classification task. However, they are all complex in structure (not end-to-end) and difficult to train (owing to instability) (Pourpanah et al. 2020). The lack of region-attribute supervision data also makes it difficult to accurately understand the corresponding relationship of different attribute-feature pairs during training.

Recently, some **Attention-based** methods begin to explore the discriminative region features guided by attentive semantic information. Specifically, RGEN (Xie et al. 2020) devises the attention technique to construct a region graph for transferring knowledge among different classes. GEM-ZSL (Liu et al. 2021b) utilizes gaze embedding to improve the localization of discriminative attributes. MSDN (Chen et al. 2022b) incorporates mutually visual-attribute attention sub-net for semantic distillation, while TransZero (Chen et al. 2022a) further extends MSDN via improving the attention layers by transformers. However, they are still confused by the universal phenomena of the attribute imbalance and co-occurrence (2019; 2021a), as shown in Figure 1. Meanwhile, the scope and availability of the input knowledge limit the performance of these models on ZSL.

In contrast to these methods, we leverage the semantic knowledge in PLMs, and design a cross-modal semantic grounding network to encourage the model to separate

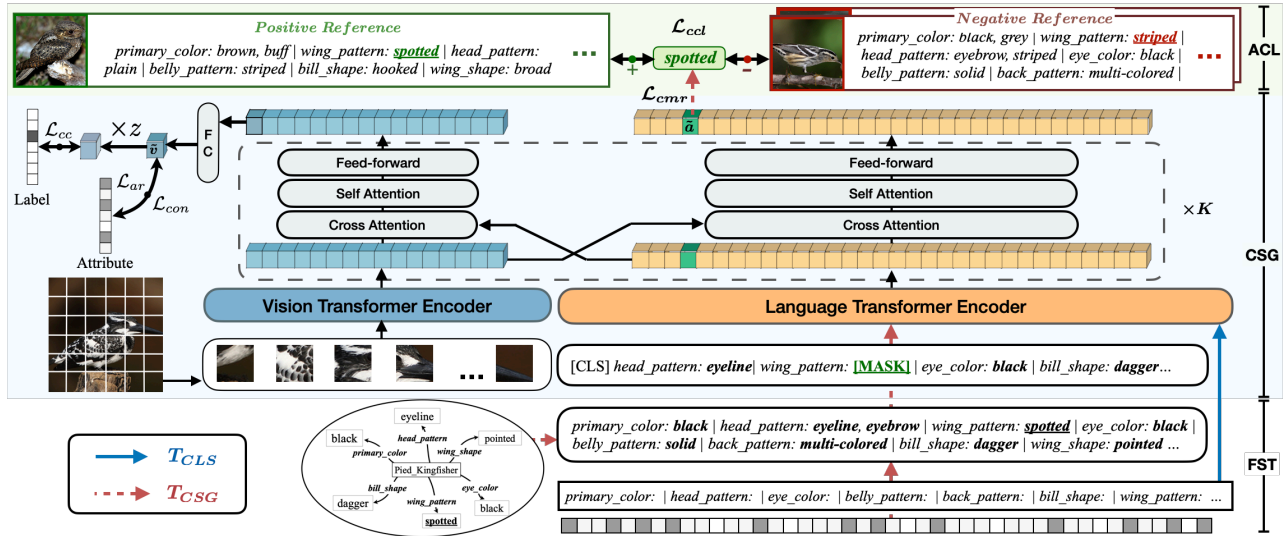


Figure 3: DUET consists of three parts: (1) a *Feature-to-sequence transformation (FST) module* which unifies attributes of each class into a textual format; (2) a *Cross-modal semantic grounding (CSG) module* which enables the knowledge transfer from PLM to vision transformer encoder via cross-modal mask reconstruction (CMR); and (3) a *Attribute-level contrastive learning (ACL) module* which enhances the signal in CSG in a self-supervised manner.

those attributes from images. Furthermore, we develop an attribute-level contrastive learning mechanism to address the attribute imbalance and co-occurrence issues, which further enhances the model’s discrimination of different independent characteristics in a self-supervised manner.

3 Methodology

Let $\mathcal{D}_s = \{(x^s, y^s) | x^s \in \mathcal{X}^s, y^s \in \mathcal{Y}^s\}$ be the training set, where x^s is an image with label y^s attached, and $\mathcal{D}_u = \{(x^u, y^u) | x^u \in \mathcal{X}^u, y^u \in \mathcal{Y}^u\}$ be the unseen dataset, where \mathcal{Y}^u and \mathcal{Y}^s are disjoint. Each label y corresponds to a class $c \in \mathcal{C} = \mathcal{C}^s \cup \mathcal{C}^u$. Specifically, ZSL aims to recognize images of unseen classes (\mathcal{C}^u) by transferring learned knowledge from seen classes (\mathcal{C}^s) using their semantic information (e.g., attributes). In this study, we assume attributes annotated to classes are given, where each attribute is sometimes associated with a real or binary value for indicating its degree. All the attributes of a dataset are denoted as $\mathcal{A} = \{a_1, \dots, a_{|\mathcal{A}|}\}$, and the attributes of a class c is denoted as $z^c = [z_1^c, \dots, z_{|\mathcal{A}|}^c]^\top$.

3.1 Feature-to-Sequence Transformation

This module unifies attributes of each class into a textual format. For ZSL datasets with binary format attributes, we assume $a_i \in \mathcal{A}$ is in the attribute set \mathcal{A}^c of class c if $z_i^c = 1$. Specifically, we propose a prompt-based policy to semi-serialize these discrete attributes to accommodate the sequential inputs of PLMs, inspired by the structured tabular data pre-training (2020; 2022). Concretely, we cluster fine-grained attributes to define k class-specific prompt (Liu et al. 2021a) set \mathcal{P} (i.e., abstract attribute set) where $\mathcal{A} = \mathcal{P}_1 \cup \dots \cup \mathcal{P}_k$. Then, given a class c , we semi-serialize its attributes with prompt (name) put ahead of each \mathcal{P}^c , and take special symbol “|” for prompt set separation. Taking the

encoded attribute sentence $\hat{\mathcal{A}}^c$ for the class “Otter” in AWA2 (2019) dataset as an example:

$$\dots | \underbrace{\text{color}}_{\text{Prompt}}: \underbrace{\text{brown}}_{\text{Attribute}} | \underbrace{\text{haspart}}_{\text{Prompt}}: \underbrace{\text{tail, flippers, } \dots}_{\text{Attributes}} | \dots \quad (1)$$

Obviously, compared to annotating large-scale fine-grained attributes for each image, it is easier to cluster limited attribute names. Since many ZSL datasets already have their incipient attribute divisions such as SUN (2012), we just need to make little adjustments like removing the repeated prefixes (e.g., “has”) and revising some ambiguous \mathcal{P} (see Appendix for details). For knowledge-based ZSL (a.k.a. K-ZSL) datasets such as AWA2-KG in OntoZSL (2021a), given a triple (c, rel, a) , e.g., $(Zebra, hasPart, Four.legs)$, we simply take the relation rel as the prompt of attribute a .

3.2 Cross-modal Semantic Grounding

This module enables the knowledge transfer from the PLM to the vision transformer encoder via attribute phrase masking and cross-modal mask reconstruction.

Attribute Phrase Masking (APM). We apply such an APM strategy to mask a complete attribute phrase at each step and then urge the model to recover it. We think *discriminative attributes with low frequency within the attribute collection are more important*. Therefore, we sample the target attribute a_t to be masked via a linear weighted random sampling (LWRS) strategy: $a_t = LWRS(\mathcal{A})$. Specifically, given a class c , the probability for sampling attribute a_j as the a_t^c is:

$$P(a_t = a_j | \mathcal{A}^c) = \frac{w_j}{\sum_{a_i \in \mathcal{A}^c} w_i}, \quad w_j = \frac{1}{\sum_{c' \in \mathcal{C}^s} \mathbb{I}[a_j \in \mathcal{A}^{c'}]}, \quad (2)$$

where $\mathbb{I}[a_j \in \mathcal{A}^{c'}]$ is an indicator function (i.e., it is 1 when $a_j \in \mathcal{A}^{c'}$, otherwise 0).

Since the scale of non-repetitive attribute sentence \hat{A} is normally much smaller than \mathcal{X}^s (i.e., $|\mathcal{C}^s| \ll |\mathcal{X}^s|$), we propose random attributes pruning (**RAP**) over the \mathcal{A}^c to remove part of the attributes (except a_t) toward a class within each training step. Specifically, we denote $\mathcal{A}_{rap} = RAP(r_{rap}, \mathcal{A})$ with hyperparameter r_{rap} as the pruning ratio. This will make the model to *recover the attribute based on relevant visual information rather than trickily utilizing attribute co-occurrence*. Thus, the masked attribute sentence constructed based on \mathcal{A}_{rap} , denoted as $\hat{\mathcal{A}}_{rap \setminus t}$, is the input of PLM encoder.

Cross-modal Mask Reconstruction (CMR). We leverage the transformer architecture to encode both the visual features and textual attributes. Specifically, we split an image x (in class c) into patches sequence and feed them into the vision transformer encoder with 1-D position embedding attached. Meanwhile, a learnable embedding v_{cls} (marked with [CLS]) is prepended whose state at the output serves as the representation of the image. Subsequently, as shown in Figure 3, K cross attention layers are stacked behind the parallel encoders for cross-modal information transfer. Each of them consists of one bi-directional cross-attention block, two self-attention blocks and two feed-forward blocks. A residual connection and layer normalization are added behind each block. The keys and values (Vaswani et al. 2017) from each modality are passed as the input to other modality’s multi-headed attention blocks. Let \tilde{v} and \tilde{a} be the output representation of image x and the masked target attribute, respectively. The objective for CMR is

$$\mathcal{L}_{cmr} = \mathbb{E}_{x \sim \mathcal{X}^s} [-z_{a_t} \sum_{i=1}^{Len(w)} \log P(w_i | \hat{\mathcal{A}}_{rap \setminus t}, x)], \quad (3)$$

where w represents the token sequence of target attribute a_t in PLM’s vocabulary \mathcal{V} , Specifically, z_{a_t} is the expressive degree score for attribute a_t in class c , which *adaptively gives more weights to those highly confident attributes* (i.e., conspicuous characteristics in a class). Moreover, we denote

$$P(w_i | \hat{\mathcal{A}}_{rap \setminus t}, x) = \exp(\tilde{a}_i \cdot e_{w_i}) / \sum_{w' \in \mathcal{V}} \exp(\tilde{a}_i \cdot e_{w'}), \quad (4)$$

where e_w refers to the token embedding of w .

Basic ZSL Classification. Following (2020b; 2022a; 2020), we present the attribute regression loss \mathcal{L}_{ar} to encourage DUET to accurately map the image representation into corresponding attribute embedding:

$$\mathcal{L}_{ar} = \mathbb{E}_{x \sim \mathcal{X}^s} \|\tilde{v} - z\|_2^2, \quad (5)$$

where z is the class-level attribute vector for image x . Meanwhile, we utilize the cross-entropy loss to enforce the image to have the highest compatibility score with its corresponding class semantic vector:

$$\mathcal{L}_{cc} = \mathbb{E}_{x \sim \mathcal{X}^s} [-\log \frac{\exp(\tilde{v} \cdot z)}{\sum_{\hat{c} \in \mathcal{C}^s} \exp(\tilde{v} \cdot z^{\hat{c}})}]. \quad (6)$$

To further strengthen DUET’s discriminative ability towards different classes with limited samples, we define a class-level supervised contrastive loss:

$$\mathcal{L}_{con} = \mathbb{E}_{x \sim \mathcal{X}^s} [-\log f_\theta(\tilde{v} | s, x)], \quad (7)$$

where s is the input sentence on language side. Specifically, let \tilde{v}^+ be the representation of positive image which has the same class label as \tilde{v} , those features with distinct label inside the mini-batch make up a negative samples $\mathcal{N}(\tilde{v})$. We define $f_\theta(\tilde{v} | s, x)$ as:

$$f_\theta = \frac{\exp(D(\tilde{v}, \tilde{v}^+)/\tau)}{\exp(D(\tilde{v}, \tilde{v}^+)/\tau) + \sum_{\tilde{v}' \in \mathcal{N}(\tilde{v})} \exp(D(\tilde{v}, \tilde{v}')/\tau)}, \quad (8)$$

where τ is the temperature hyper-parameter. $D(\tilde{v}, \tilde{v}^+)$ denotes the cosine similarity between $H(\tilde{v})$ and $H(\tilde{v}^+)$, where $H(\cdot)$ is a non-linear projection head (Chen et al. 2020).

Multi-task Learning. As the core part of cross-modal semantic grounding (CSG), the multi-task learning procedure (2018; 2021) forces the model to spread attribute information between the vision side and the language side via a task switching strategy. Namely, DUET conducts CMR at stage T_{CSG} by accessing the visual patches and $\hat{\mathcal{A}}_{rap}$, and conducts simple image classification task at stage T_{CLS} without seeing the textual attributes. Specifically, the input sequence s_{tmp} at T_{CLS} is fixed as the prompt template to mimic the single-modal testing phase:

$$\dots | \underbrace{\text{color}}_{\text{Prompt}} : | \underbrace{\text{haspart}}_{\text{Prompt}} : | \underbrace{\text{pattern}}_{\text{Prompt}} : | \underbrace{\text{shape}}_{\text{Prompt}} : | \dots \quad (9)$$

Let L_{CLS} , L_{CSG} be the loss function of basic ZSL classification and CSG, respectively. At each step, we apply the objective L_{CLS} (for T_{CLS}) with probability $1 - \rho$, or L_{CSG} (for T_{CSG}) with probability ρ :

$$L_{CLS} = \mathcal{L}_{zsl} + \lambda_{con} \mathcal{L}_{con}, \quad (10)$$

$$L_{CSG} = \mathcal{L}_{zsl} + \lambda_{cmr} \mathcal{L}_{cmr}, \quad (11)$$

where we denote $\mathcal{L}_{zsl} = \mathcal{L}_{cc} + \lambda_{ar} \mathcal{L}_{ar}$ as the ‘‘ZSL loss’’.

3.3 Attribute-level Contrastive Learning

To further strengthen the model’s sensitivity on subtle visual differences against the attribute co-occurrences, we introduce an attribute-level contrastive learning (ACL) module with the adaptive loss function:

$$\mathcal{L}_{acl} = \mathbb{E}_{x \sim \mathcal{X}^s} [-\text{Min}(z_a, z_{a^+}) \log f_\phi(\tilde{a} | s, x)], \quad (12)$$

where $f_\phi(\tilde{a} | s, x)$ follows the base formulation of Eq. (8), but there are 3 main differences between f_ϕ and f_θ :

(i) *Target Object and Stage.* f_ϕ targets at the mean-pooling representation of \tilde{a} on language side of stage T_{CSG} , where the input sentence s is $\hat{\mathcal{A}}_{rap \setminus t}$. While f_θ targets at the feature (\tilde{v}) on vision side, which is applied at stage T_{CLS} with a fixed prompt template (9) as the s_{tmp} .

(ii) *Sampling Strategy.* For class-level f_θ , we simply pick those images, which share the same class label with original sample as positive, and then define the rest as in-batch negative. While for attribute-level f_ϕ , we design an attribute-based sampling strategy: Given a class c and its target attribute a_t^c , we assume $a_t^{c^-}$ as the negative attribute from seen class c^- , and $a_t^{c^+}$ as the positive attribute from seen class c^+ . We claim the precondition as:

$$c \neq c^+ \neq c^-, a_t^c = a_t^{c^+} \neq a_t^{c^-}, \quad (13)$$

$$a_t^c, a_t^{c^-} \in \mathcal{P}_t, a_t^{c^-} \notin \mathcal{P}_t^c, a_t^c \notin \mathcal{P}_t^{c^-}, \quad (14)$$

Table 1: Results (%) of our method and the baselines. † and * indicate generative methods and non-generative methods, respectively. The best results in baselines are marked with underline, and we highlight our results with **bold** when we achieve new SOTA. For CZSL, results are reported with the top-5 classification accuracy (T1). For GZSL, results are reported in terms of T1 accuracy of unseen (U) and seen (S) classes, together with their harmonic mean (H) where $H = (2 \times S \times U)/(S + U)$.

Methods	CUB				SUN				AWA2			
	CZSL T1	GZSL			CZSL T1	GZSL			CZSL T1	GZSL		
		U	S	H		U	S	H		U	S	H
† TF-VAEGAN (ECCV) (2020)	64.9	52.8	64.7	58.1	<u>66.0</u>	45.6	40.7	43.0	72.2	59.8	75.1	66.6
Composer (NeurIPS) (2020a)	69.4	56.4	63.8	59.9	62.6	<u>55.1</u>	22.0	31.4	71.5	62.1	77.3	68.8
CE-GZSL (CVPR) (2021)	77.5	63.1	66.8	65.3	63.3	48.8	38.6	43.1	70.4	63.1	78.6	70.0
GCM-CF (CVPR) (2021)	–	61.0	59.7	60.3	–	47.9	37.8	42.2	–	60.4	75.1	67.0
FREE (ICCV) (2021c)	–	55.7	59.9	57.7	–	47.4	37.2	41.7	–	60.4	75.4	67.1
HSVA (NeurIPS) (2021d)	62.8	52.7	58.3	55.3	63.8	48.6	39.0	<u>43.3</u>	–	59.3	76.6	66.8
AGZSL (ICLR) (2021)	57.2	41.4	49.7	45.2	63.3	29.9	40.2	34.3	<u>73.8</u>	65.1	78.9	71.3
* APN (NeurIPS) (2020)	72.0	65.3	69.3	67.2	61.6	41.9	34.0	37.6	68.4	57.1	72.4	63.9
DVBE (CVPR) (2020)	–	53.2	60.2	56.5	–	45.0	37.2	40.7	–	63.6	70.8	67.0
DAZLE (CVPR) (2020b)	66.0	56.7	59.6	58.1	59.4	52.3	24.3	33.2	67.9	60.3	75.7	67.1
RGEM (ECCV) (2020)	76.1	60.0	<u>73.5</u>	66.1	63.8	44.0	31.7	36.8	73.6	<u>67.1</u>	76.5	71.5
GEM-ZSL (CVPR) (2021b)	<u>77.8</u>	64.8	69.3	67.2	62.8	38.1	35.7	36.9	67.3	64.8	77.5	70.6
MSDN (CVPR) (2022b)	76.1	68.7	67.5	68.1	65.8	52.2	34.2	41.3	70.1	62.0	74.5	67.7
TransZero (AAAI) (2022a)	76.8	<u>69.3</u>	68.3	<u>68.8</u>	65.6	52.6	33.4	40.8	70.1	61.3	<u>82.3</u>	70.2
DUET (Ours)	72.3	62.9	72.8	67.5	64.4	45.7	45.8	45.8	69.9	63.7	84.7	72.7

where \mathcal{P}_t is the original class-agnostic prompt set that a_t belongs to, and $\mathcal{P}_t^c, \mathcal{P}_t^{c^-}$ is the class-specific prompt set in class c, c^- . All c^+, c^- that satisfies this precondition make up the candidate class set \mathcal{C}^+ and \mathcal{C}^- , respectively.

(iii) *Sampling Probability*. We employ a heuristic process to let the model select those c^+ whose \mathcal{A}^{c^+} are more *inconsistent*, and c^- whose \mathcal{A}^{c^-} are more *similar*, compared with \mathcal{A}^c (see Appendix). Then, we non-repetitively choose instances (i.e. x^{c^-} and x^{c^+}) from these classes, and encode them by DUET to get the final \tilde{a}^- and \tilde{a}^+ . Note that $a_t^{c^-}$ and $a_t^{c^+}$ are not masked to accelerate the convergence.

Finally, we stack this pluggable ACL module into CSG:

$$L_{CSG} \leftarrow L_{CSG} + \mathcal{L}_{acl}. \quad (15)$$

Remark 1 *Considering the example in Figure 1, we assume “Pied Kingfisher” as the original bird class (c) with target attribute “spotted” (a_t) in the prompt set “wing pattern” (\mathcal{P}_t^c). We are likely to sample “Chuck will’s widow” as the positive class c^+ which contains spotted wing pattern, but has a low class similarity (28.6% after normalization) compared with “Pied Kingfisher”. Besides, we prefer to sample “Black-and-white Warbler” as the negative class c^- whose wing pattern is striped (not “spotted”) but the class characteristic is pretty closed (73.8%) to “Pied Kingfisher”.*

3.4 Zero-Shot Prediction

After training DUET, we use the learned cosine metric space for zero-shot recognition. There are two evaluation settings: conventional ZSL (CZSL), which classifies the testing samples with candidate classes from \mathcal{C}^u ; generalized ZSL (GZSL), which extends the candidate classes to $\mathcal{C}^s \cup \mathcal{C}^u$. Specifically, we take the prompt template s_{tmp} together with an test image x as the input. Following (2022a; 2021b; 2022b), we predict the label c^* via:

$$c^* = \arg \max_{c \in \mathcal{C}^u / \mathcal{C}} (\tilde{v} \cdot z^c) - \gamma \mathbb{I}[c \in \mathcal{C}^s], \quad (16)$$

where $\mathbb{I} = 1$ if c is a seen class and 0 otherwise. γ is the calibration factor tuned on a held-out validation set, and $\mathcal{C}^u / \mathcal{C}$ corresponds to the CZSL/GZSL setting respectively.

4 Experiments

4.1 Datasets

We select three standard attribute equipped ZSL benchmarks **AWA2** (2019), **CUB** (2010), **SUN** (2012) with their splits proposed in (2019), as well as a knowledge graph equipped benchmark **AWA2-KG** which has the same split as AWA2 but includes semantic information about hierarchical classes and attributes, for evaluation. In AWA2-KG, we assume that the class c has the attribute a_i when the length of the shortest same-direction relation path between them in KG is h , where h is a hyperparameter. For example, given two triples (*Zebra, hasPart, Four_legs*) and (*Four_legs, subclassOf, Leg*), the attribute of class “Zebra” is “Four_leg” when $h=1$ and “Leg” when $h=2$. Since we observe that the attribute a become more coarse-grained when they are far away from the class c in KG, we simply define h as 1. Please see Appendix for detailed statistics of all datasets.

Besides, there are also some other ZSL datasets like aPY (2009) and AWA1 (2014). We do not evaluate on them since most of their unseen classes are leakage (Xian et al. 2019) in ImageNet-1K (2009), which is a common image datasets for normal vision encoder pre-training.

4.2 Experimental Settings

Unlike previous ZSL studies which pre-extract the image features using a pre-trained CNN model e.g., ResNet (2016), we take as input the raw images and apply vision transformer to interact with the PLM for knowledge transfer. For those coefficients in AWA2, we set λ_{ar} to 0.01, λ_{con} to 0.05, λ_{cmr} to 1, λ_{acl} to 0.01, r_{rap} to 0.5, ρ to 0.4 and γ to 0.8. Please see Appendix for details about the backbones choosing and

hyperparameters setting in all datasets. We report the class-averaged (macro) accuracy as the basic metric, following the current literature (Xu et al. 2020; Chen et al. 2022a).

4.3 Overall Results

Standard ZSL Datasets. We compare our method with 14 representative or state-of-the-art (SOTA) methods proposed in recent three years. These baselines are divided into two categories: non-generative (2020; 2020; 2020b; 2020; 2021b; 2022b; 2022a) and generative (2020; 2020a; 2021; 2021; 2021c; 2021d; 2021). All those non-generative methods are attention-based except for DVBE (Min et al. 2020).

SUN contains more than 700 scene classes but each class has only 10-20 images instances, where the attribute imbalance and co-occurrence problem are universal. We find that DUET achieves the best accuracy (45.8%) on H with a large margin (2.5%) compared with those SOTA methods, and surpass MSDN (Chen et al. 2022b) by 4.5% on H , which is the SOTA no-generative methods on SUN. On **AWA2**, DUET gains 1.2% improvements over the SOTA performance, and outperforms the transformer-based method TransZero (2022a) on all the GZSL metrics.

On **CUB**, DUET achieves competitive performance, surpassing all generative methods on H , except for the attention-based methods TransZero and MSDN. We own this to the fact that the prompts in CUB are mostly region-related (e.g., “breast_color” and “wing_color”), but DUET simply attaches the image patches with sequential 1-dimensional positional embedding as the input, making it hard to capture the fine-grained positional relationship. Instead, TransZero takes 2D center coordinates to construct learnable relative region geometric embeddings for feature augmentation, which gets accurate position representations and helps the model achieve good performance. Notably, when it does not use feature augmentation from relative geometry relationships, the H on CUB dramatically decreases to 66.5% (Chen et al. 2022a).

It is worth mentioning that DUET also achieves great performance on seen classes (S) on all three datasets, outperforming all baselines on SUN and AWA2 by at least 5.1% and 2.4% respectively. This proves that DUET well preserves the predictive ability on seen classes in addressing unseen classes.

K-ZSL Dataset. We evaluate on AWA2-KG (Geng et al. 2021a) to validate DUET’s flexibility on various ZSL attribute formats. Specifically, we pick the KG from (Geng et al. 2021b) as the knowledge resource, and compare with other applicable baselines including DeVISE (2013), SYNC (2016), DGP (2019), LsrGAN[†] (2020). We abandon the real-value attributes for fairness, and follow (2021a; 2022; 2021e) to take the KG embedding (2013) for entity class representation toward \mathcal{L}_{ar} and \mathcal{L}_{cc} . As shown in Figure 4(a), DUET achieves higher performance among all other methods. In particular, it achieves a 30.2% improvement on metric H compared to the non-generative method DGP.

ViT-based DUET. To get further insights into our model, we report the results of DUET with ViT-base (2021) as the vision encoder. Remarkably, since the released ViT-base is

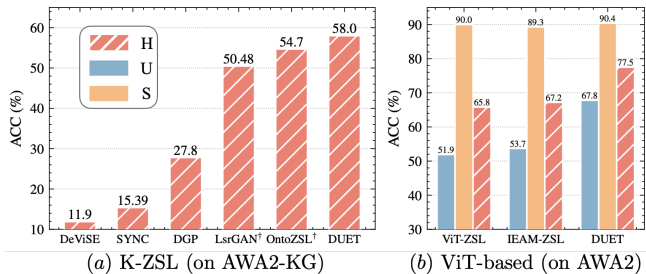


Figure 4: (a) Results (%) on AWA2-KG from OntoZSL. The attribute values in this dataset are all represent in 0/1 binary form. We marks those generative methods with “†”. (b) Results (%) on AWA2 with ViT-base as the vision encoder.

pre-trained on ImageNet-21K which may contain unseen objects, we only select 2 recent ViT-based ZSL methods, ViT-ZSL (2021) and IEAM-ZSL (2020), for comparison. As shown in Figure 4(b), DUET surpasses these two methods by a large margin (14.1% improvement on U and 10.3% improvement on H) and also exceeds our SOTA performance (H) by 4.8%. This supports that our DUET greatly ameliorates the ZSL ability where the original vision transformer is poor. We believe that the performance will be further improved by plugging in a better vision transformer encoder.

4.4 Ablation Studies

Table 2: Results (%) of ablation studies on AWA2 by GZSL. The metric is harmonic mean (H) accuracy. Δ indicates the performance drop compared with our full model.

Methods	H	Δ
Only ENC_{vis}	64.1	8.6↓
1) CSG _{freeze ENC_{lan}}	66.5	6.2↓
2) CSG _{w/ only Prompt}	61.7	11.0↓
3) CSG _{w/o Prompt}	64.9	7.8↓
4) CSG _{w/o LWRs}	66.9	5.8↓
5) CSG _{w/o RAP}	67.4	5.3↓
6) CSG _{w/o \mathcal{L}_{con}}	68.4	4.3↓
7) CSG	69.2	3.5↓
DUET (Full model)	72.7	-

Component Analysis. To prove that our improvement in performance is not just from the Vision Transformer ENC_{vis} , we evaluate various stripped-down versions of our proposed model to compare the (H) performance gain brought by different components on AWA2. Concretely, we observe that the performance drops sharply when (1) freezing the language transformer encoder ENC_{lan} . Although it can reduce the overall learnable parameters, it makes the model harder to understand the special relationship among prompts, textual attributes, and visual features. From the results of taking (2) only the prompt and (3) only concatenating attribute as sequence input without the prompt, we observe that employing our FST strategy for semi-serializing attributes indeed benefits our model with 4.3% improvement. We also exploit the influence of (4) randomly masking attributes, (5) not conducting attribute pruning, which leads to 2.3%, 1.8% falls compared with (7) applying the full

CSG, proving the necessity of both sampling target attribute with adaptive weight and pruning part of the attribute. Besides, (6) abandoning class-level contrastive learning leads to 0.8% decrease. We own this to the fact that contrastive learning can help model learn better visual representations by narrowing the distance within a class in the latent space. Most importantly, our pluggable ACL module further boosts the performance by 3.5% based on CSG, which illustrates that both of these modules are beneficial.

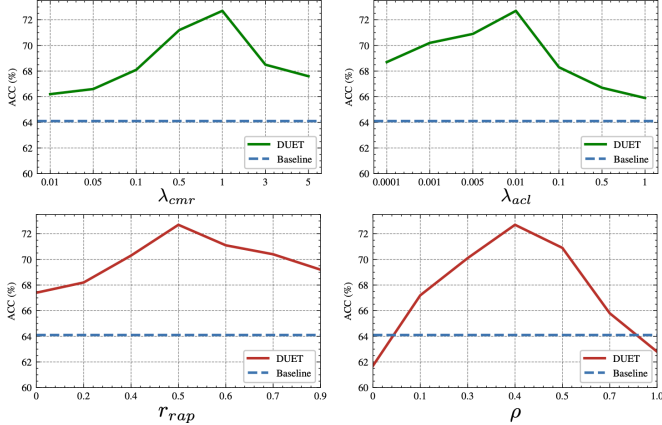


Figure 5: A parameter analysis of coefficients λ_{cmr} , λ_{acl} , r_{rap} (the pruning ratio for $RAP(\cdot)$), ρ (the probability for employing L_{CSG}). Baseline denotes the pure vision transformer encoder. H accuracy on AWA2 is reported.

Hyperparameter Analysis. By comparing DUET’s performance in Figure 5, we conclude that: (i) The performance decrease when λ_{cmr} and λ_{acl} are too large, since the weak signal from the self-supervised objectives (i.e., \mathcal{L}_{cmr} and \mathcal{L}_{acl}) will gradually overwhelm the signal from supervised class label (i.e., \mathcal{L}_{ar} and \mathcal{L}_{cc}). (ii) When ρ is close to 1 or 0, the protocol all drops below the baseline. This is because the model turns into a single-modal task without multi-task learning when $\rho = 0$. While when $\rho = 1$, DUET is forced to classify the image with attribute attached throughout the training, leading to model’s poor generalization capability at test stage. (iii) Furthermore, we try a wide range of r_{rap} , i.e. $r_{rap} = \{0, 0.2, 0.4, 0.5, 0.6, 0.7, 0.8\}$, and find that DUET works best when r_{rap} is set to 0.5.

4.5 Interpretation

To prove DUET’s capability on disentangling image-specific semantic attributes, we feed an image into the well-trained DUET together with a crafted template: “...| \hat{P} : [MASK]|...”, where each prompt name \hat{P} is involved with the [MASK] followed to recover attribute tokens (see Appendix for more details). Figure 6 shows the prediction results from the cases in SUN’s testing set. We observe that DUET can successfully retrieve most relevant attributes from the image given a concrete prompt, e.g., the “sport” function from a “basketball arena” and the “natural” light from an open-air “bus depot”.

Sometimes, there also exist unreasonable attribute pairs within a class in GT attribute sets. For example, (i) “oilrig”

Image Case	Prompt	Attribute
	transportation function	DUET: boating (46.60%) swimming (34.39%) digging (19.01%)
		GT: boating (51.99%) swimming (12.71%)
	coarse material	DUET: metal (39.91%) ocean (37.55%) wire (22.54%)
		GT: ocean (48.52%) metal (43.90%) wire (6.93%)
	environment function	DUET: reading (55.42%) eating (31.13%) working (13.45%)
		GT: reading (46.60%) eating (12.33%) socializing (6.85%)
	specific material	DUET: cloth (39.55%) flowers (38.47%) tiles (21.98%)
feeling	GT: carpet (28.78%) cloth (23.30%) flowers (10.96%)	
	DUET: soothing (59.97%) symmetrical (32.92%) cluttered (7.11%)	
	environment function	DUET: sports (49.15%) playing (32.78%) socializing (18.07%)
		GT: congregating (47.31%) sports (43.48%) playing (11.51%)
	technical function	DUET: competing (40.00%) audience (36.19%) exercise (23.81%)
		GT: competing (52.43%) audience (52.43%) exercise (17.90%)
	surface	DUET: glossy (41.56%) rusty (32.74%) sterile (25.70%)
	transportation function	DUET: driving (42.95%) biking (37.98%) climbing (19.07%)
		GT: driving (41.53%) biking (17.96%)
	coarse material	DUET: asphalt (34.28%) metal (33.71%) concrete (32.01%)
		GT: asphalt (38.94%) metal (22.06%) pavement (20.77%)
light	DUET: natural (57.30%) indoor (33.55%) direct sun/sunny (9.15%)	
	GT: natural (54.51%) direct sun/sunny (20.36%)	

Figure 6: Attribute prediction for interpretation.

has both “still water” and “waves” as its attributes, which is *contradictory*; (ii) there is no “carpet” in this “living room” image, but it has high confidence. These situations occur when mutually exclusive attributes are independently contained in different images within the same class, since the class-level attribute values in SUN are collected by averaging the binary labels from annotators. In contrast, our DUET could achieve *instance-level semantic grounding*, correctly giving “waves” high score in this “oilrig”, and ignoring “carpet” in this “living room”.

Besides, the scarce attribute “fire” is confidently predicted in the “oilrig” image, while in “living room”, the “flowers” are recovered without “leaves” bound together, which demonstrate the capability of DUET in *addressing the attribute imbalance and attribute co-occurrence issues* shown in Figure 1. Moreover, DUET can ground not only obvious visual attributes (e.g., “fire”) but also those abstract properties (e.g., “soothing” for “feeling” and “competing” for “technical function”), which shows its potential capability for knowledge inference.

5 Conclusion

In this paper we propose an end-to-end ZSL framework named DUET to incorporate the semantics from a PLM into a vision transformer encoder via a self-supervised multi-modal learning paradigm. We design a cross-modal semantic grounding network with a novel attribute-level contrastive learning mechanism to enhance the model’s discriminative ability towards novel classes, which could well address the issues of attribute imbalance and co-occurrence in zero-shot image classification. With extensive ablation studies and the comparison with quite a few state-of-the-art methods on four ZSL benchmarks with real-valued and binary-valued attributes, we demonstrate the effectiveness of DUET as well as its support for interpretation.

References

- Alamri, F.; and Dutta, A. 2021. Multi-Head Self-Attention via Vision Transformer for Zero-Shot Learning. *CoRR*, abs/2108.00045. 4.3
- Bao, H.; Dong, L.; and Wei, F. 2021. BEiT: BERT Pre-Training of Image Transformers. *CoRR*, abs/2106.08254. A.7
- Bordes, A.; Usunier, N.; García-Durán, A.; Weston, J.; and Yakhnenko, O. 2013. Translating Embeddings for Modeling Multi-relational Data. In *NIPS*, 2787–2795. 4.3
- Changpinyo, S.; Chao, W.-L.; Gong, B.; and Sha, F. 2016. Synthesized classifiers for zero-shot learning. In *Proceedings of the IEEE conference on computer vision and pattern recognition*, 5327–5336. 4.3
- Chen, J.; Geng, Y.; Chen, Z.; Horrocks, I.; Pan, J. Z.; and Chen, H. 2021a. Knowledge-aware Zero-Shot Learning: Survey and Perspective. In *IJCAI*, 4366–4373. ijcai.org. 2.1
- Chen, J.; Geng, Y.; Chen, Z.; Pan, J. Z.; He, Y.; Zhang, W.; Horrocks, I.; and Chen, H. 2021b. Low-resource Learning with Knowledge Graphs: A Comprehensive Survey. *CoRR*, abs/2112.10006. 2.1
- Chen, S.; Hong, Z.; Liu, Y.; Xie, G.-S.; Sun, B.; Li, H.; Peng, Q.; Lu, K.; and You, X. 2022a. TransZero: Attribute-guided Transformer for Zero-Shot Learning. In *AAAI*. 1, 2.1, 3.2, 1, 3.4, 4.2, 4.3
- Chen, S.; Hong, Z.; Xie, G.-S.; Yang, W.; Peng, Q.; Wang, K.; Zhao, J.; and You, X. 2022b. MSDN: Mutually Semantic Distillation Network for Zero-Shot Learning. In *CVPR*. 1, 2.1, 1, 3.4, 4.3
- Chen, S.; Wang, W.; Xia, B.; Peng, Q.; You, X.; Zheng, F.; and Shao, L. 2021c. FREE: Feature Refinement for Generalized Zero-Shot Learning. In *ICCV*, 122–131. IEEE. 2.1, 1, 4.3
- Chen, S.; Xie, G.-S.; Peng, Q.; Liu, Y.; Sun, B.; Li, H.; You, X.; and Shao, L. 2021d. HSVA: Hierarchical Semantic-Visual Adaptation for Zero-Shot Learning. In *35th Conference on Neural Information Processing Systems (NeurIPS)*. 1, 2.1, 1, 4.3
- Chen, T.; Kornblith, S.; Norouzi, M.; and Hinton, G. E. 2020. A Simple Framework for Contrastive Learning of Visual Representations. In *ICML*, volume 119 of *Proceedings of Machine Learning Research*, 1597–1607. PMLR. 3.2
- Chen, Y.; and Yeh, M. 2021. Text-Enhanced Attribute-Based Attention for Generalized Zero-Shot Fine-Grained Image Classification. In *ICMR*, 447–450. ACM. 2.1
- Chen, Z.; Chen, J.; Geng, Y.; Pan, J. Z.; Yuan, Z.; and Chen, H. 2021e. Zero-Shot Visual Question Answering Using Knowledge Graph. In *ISWC*, volume 12922 of *Lecture Notes in Computer Science*, 146–162. Springer. 4.3
- Chen, Z.; Luo, Y.; Qiu, R.; Wang, S.; Huang, Z.; Li, J.; and Zhang, Z. 2021f. Semantics Disentangling for Generalized Zero-Shot Learning. In *ICCV*, 8692–8700. IEEE. 2.1
- Chen, Z.; Luo, Y.; Wang, S.; Qiu, R.; Li, J.; and Huang, Z. 2021g. Mitigating Generation Shifts for Generalized Zero-Shot Learning. In *ACM Multimedia*, 844–852. ACM. 1
- Chou, Y.; Lin, H.; and Liu, T. 2021. Adaptive and Generative Zero-Shot Learning. In *ICLR*. OpenReview.net. 1, 4.3
- Cui, Y.; Che, W.; Liu, T.; Qin, B.; and Yang, Z. 2021. Pre-Training With Whole Word Masking for Chinese BERT. *IEEE ACM Trans. Audio Speech Lang. Process.*, 29: 3504–3514. A.7
- Deng, J.; Dong, W.; Socher, R.; Li, L.; Li, K.; and Fei-Fei, L. 2009. ImageNet: A large-scale hierarchical image database. In *CVPR*, 248–255. IEEE Computer Society. 4.1, A.1
- Devlin, J.; Chang, M.; Lee, K.; and Toutanova, K. 2019. BERT: Pre-training of Deep Bidirectional Transformers for Language Understanding. In *NAACL-HLT (1)*, 4171–4186. Association for Computational Linguistics. A.2, A.7
- Dong, H.; Cheng, Z.; He, X.; Zhou, M.; Zhou, A.; Zhou, F.; Liu, A.; Han, S.; and Zhang, D. 2022. Table Pre-training: A Survey on Model Architectures, Pre-training Objectives, and Downstream Tasks. In *IJCAI*, 5426–5435. ijcai.org. 3.1
- Dosovitskiy, A.; Beyer, L.; Kolesnikov, A.; Weissenborn, D.; Zhai, X.; Unterthiner, T.; Dehghani, M.; Minderer, M.; Heigold, G.; Gelly, S.; Uszkoreit, J.; and Houshly, N. 2021. An Image is Worth 16x16 Words: Transformers for Image Recognition at Scale. In *ICLR*. OpenReview.net. 4.3, A.7, A.8
- Farhadi, A.; Endres, I.; Hoiem, D.; and Forsyth, D. A. 2009. Describing objects by their attributes. In *CVPR*, 1778–1785. IEEE Computer Society. 4.1
- Frome, A.; Corrado, G. S.; Shlens, J.; Bengio, S.; Dean, J.; Ranzato, M.; and Mikolov, T. 2013. DeViSE: A Deep Visual-Semantic Embedding Model. In *NIPS*, 2121–2129. 1, 2.1, 4.3
- Geng, Y.; Chen, J.; Chen, Z.; Pan, J. Z.; Ye, Z.; Yuan, Z.; Jia, Y.; and Chen, H. 2021a. OntoZSL: Ontology-enhanced Zero-shot Learning. In *WWW*, 3325–3336. ACM / IW3C2. 2.1, 3.1, 4.3
- Geng, Y.; Chen, J.; Chen, Z.; Pan, J. Z.; Yuan, Z.; and Chen, H. 2021b. K-ZSL: resources for knowledge-driven zero-shot learning. *arXiv preprint arXiv:2106.15047*. 4.3
- Geng, Y.; Chen, J.; Zhang, W.; Xu, Y.; Chen, Z.; Pan, J. Z.; Huang, Y.; Xiong, F.; and Chen, H. 2022. Disentangled Ontology Embedding for Zero-shot Learning. *CoRR*, abs/2206.03739. 4.3
- Han, Z.; Fu, Z.; Chen, S.; and Yang, J. 2021. Contrastive Embedding for Generalized Zero-Shot Learning. In *CVPR*, 2371–2381. Computer Vision Foundation / IEEE. 2.1, 1, 4.3
- He, K.; Chen, X.; Xie, S.; Li, Y.; Dollár, P.; and Girshick, R. B. 2021. Masked Autoencoders Are Scalable Vision Learners. *CoRR*, abs/2111.06377. A.7
- He, K.; Zhang, X.; Ren, S.; and Sun, J. 2016. Deep Residual Learning for Image Recognition. In *CVPR*, 770–778. IEEE Computer Society. 4.2
- Huynh, D.; and Elhamifar, E. 2020a. Compositional Zero-Shot Learning via Fine-Grained Dense Feature Composition. In *NeurIPS*. 2.1, 1, 4.3
- Huynh, D.; and Elhamifar, E. 2020b. Fine-Grained Generalized Zero-Shot Learning via Dense Attribute-Based Attention. In *CVPR*, 4482–4492. Computer Vision Foundation / IEEE. 3.2, 1, 4.3

- Kampffmeyer, M.; Chen, Y.; Liang, X.; Wang, H.; Zhang, Y.; and Xing, E. P. 2019. Rethinking Knowledge Graph Propagation for Zero-Shot Learning. In *CVPR*, 11487–11496. Computer Vision Foundation / IEEE. 4.3
- Lampert, C. H.; Nickisch, H.; and Harmeling, S. 2014. Attribute-Based Classification for Zero-Shot Visual Object Categorization. *IEEE Trans. Pattern Anal. Mach. Intell.*, 36(3): 453–465. 4.1
- Li, X.; Yin, X.; Li, C.; Zhang, P.; Hu, X.; Zhang, L.; Wang, L.; Hu, H.; Dong, L.; Wei, F.; Choi, Y.; and Gao, J. 2020. Oscar: Object-Semantics Aligned Pre-training for Vision-Language Tasks. In *ECCV (30)*, volume 12375 of *Lecture Notes in Computer Science*, 121–137. Springer. A.7
- Liu, P.; Yuan, W.; Fu, J.; Jiang, Z.; Hayashi, H.; and Neubig, G. 2021a. Pre-train, Prompt, and Predict: A Systematic Survey of Prompting Methods in Natural Language Processing. *CoRR*, abs/2107.13586. 3.1
- Liu, Y.; Ott, M.; Goyal, N.; Du, J.; Joshi, M.; Chen, D.; Levy, O.; Lewis, M.; Zettlemoyer, L.; and Stoyanov, V. 2019. RoBERTa: A Robustly Optimized BERT Pretraining Approach. *CoRR*, abs/1907.11692. A.7
- Liu, Y.; Zhou, L.; Bai, X.; Huang, Y.; Gu, L.; Zhou, J.; and Harada, T. 2021b. Goal-Oriented Gaze Estimation for Zero-Shot Learning. In *CVPR*, 3794–3803. Computer Vision Foundation / IEEE. 2.1, 1, 3.4, 4.3
- Liu, Z.; Lin, Y.; Cao, Y.; Hu, H.; Wei, Y.; Zhang, Z.; Lin, S.; and Guo, B. 2021c. Swin Transformer: Hierarchical Vision Transformer using Shifted Windows. In *ICCV*, 9992–10002. IEEE. A.2, A.7, A.8
- Lu, J.; Batra, D.; Parikh, D.; and Lee, S. 2019. ViLBERT: Pretraining Task-Agnostic Visiolinguistic Representations for Vision-and-Language Tasks. In *NeurIPS*, 13–23. A.7
- Min, S.; Yao, H.; Xie, H.; Wang, C.; Zha, Z.; and Zhang, Y. 2020. Domain-Aware Visual Bias Eliminating for Generalized Zero-Shot Learning. In *CVPR*, 12661–12670. Computer Vision Foundation / IEEE. 1, 4.3
- Naeem, M. F.; Xian, Y.; Tombari, F.; and Akata, Z. 2021. Learning Graph Embeddings for Compositional Zero-Shot Learning. In *CVPR*, 953–962. Computer Vision Foundation / IEEE. 2.1
- Narayan, S.; Gupta, A.; Khan, F. S.; Snoek, C. G. M.; and Shao, L. 2020. Latent Embedding Feedback and Discriminative Features for Zero-Shot Classification. In *ECCV (22)*, volume 12367 of *Lecture Notes in Computer Science*, 479–495. Springer. 1, 4.3, 4.3
- Nawaz, S.; Cavazza, J.; and Bue, A. D. 2022. Semantically Grounded Visual Embeddings for Zero-Shot Learning. *CoRR*, abs/2201.00577. A.7
- Patterson, G.; and Hays, J. 2012. SUN attribute database: Discovering, annotating, and recognizing scene attributes. In *CVPR*, 2751–2758. IEEE Computer Society. 1, 3.1, 4.1, A.1
- Pourpanah, F.; Abdar, M.; Luo, Y.; Zhou, X.; Wang, R.; Lim, C. P.; and Wang, X. 2020. A Review of Generalized Zero-Shot Learning Methods. *CoRR*, abs/2011.08641. 2.1
- Sener, O.; and Koltun, V. 2018. Multi-Task Learning as Multi-Objective Optimization. In *NeurIPS*, 525–536. 3.2
- Tan, H.; and Bansal, M. 2019. LXMERT: Learning Cross-Modality Encoder Representations from Transformers. In *EMNLP/IJCNLP (1)*, 5099–5110. Association for Computational Linguistics. A.7
- Touvron, H.; Cord, M.; Douze, M.; Massa, F.; Sablayrolles, A.; and Jégou, H. 2021. Training data-efficient image transformers & distillation through attention. In *ICML*, volume 139 of *Proceedings of Machine Learning Research*, 10347–10357. PMLR. A.2, A.7, A.8
- Vaswani, A.; Shazeer, N.; Parmar, N.; Uszkoreit, J.; Jones, L.; Gomez, A. N.; Kaiser, L.; and Polosukhin, I. 2017. Attention is All you Need. In *NIPS*, 5998–6008. 3.2, A.7
- Vyas, M. R.; Venkateswara, H.; and Panchanathan, S. 2020. Leveraging seen and unseen semantic relationships for generative zero-shot learning. In *European Conference on Computer Vision*, 70–86. Springer. 4.3
- Wang, L.; Huang, J.; Li, Y.; Xu, K.; Yang, Z.; and Yu, D. 2021a. Improving Weakly Supervised Visual Grounding by Contrastive Knowledge Distillation. In *CVPR*, 14090–14100. Computer Vision Foundation / IEEE. 1, 2.1
- Wang, W.; Xie, E.; Li, X.; Fan, D.; Song, K.; Liang, D.; Lu, T.; Luo, P.; and Shao, L. 2021b. Pyramid Vision Transformer: A Versatile Backbone for Dense Prediction without Convolutions. In *ICCV*, 548–558. IEEE. A.7
- Welinder, P.; Branson, S.; Mita, T.; Wah, C.; Schroff, F.; Belongie, S.; and Perona, P. 2010. Caltech-UCSD birds 200. 4.1, A.1
- Whitehead, S.; Wu, H.; Ji, H.; Feris, R.; and Saenko, K. 2021. Separating Skills and Concepts for Novel Visual Question Answering. In *CVPR*, 5632–5641. Computer Vision Foundation / IEEE. 3.2
- Xian, Y.; Lampert, C. H.; Schiele, B.; and Akata, Z. 2019. Zero-Shot Learning - A Comprehensive Evaluation of the Good, the Bad and the Ugly. *IEEE Trans. Pattern Anal. Mach. Intell.*, 41(9): 2251–2265. 3.1, 4.1, A.1
- Xie, G.; Liu, L.; Zhu, F.; Zhao, F.; Zhang, Z.; Yao, Y.; Qin, J.; and Shao, L. 2020. Region Graph Embedding Network for Zero-Shot Learning. In *ECCV (4)*, volume 12349 of *Lecture Notes in Computer Science*, 562–580. Springer. 2.1, 1, 4.3
- Xu, W.; Xian, Y.; Wang, J.; Schiele, B.; and Akata, Z. 2020. Attribute Prototype Network for Zero-Shot Learning. In *NeurIPS*. 3.2, 1, 4.2, 4.3
- Yin, P.; Neubig, G.; Yih, W.; and Riedel, S. 2020. TaBERT: Pretraining for Joint Understanding of Textual and Tabular Data. In *ACL*, 8413–8426. Association for Computational Linguistics. 3.1, A.7
- Yue, Z.; Wang, T.; Sun, Q.; Hua, X.; and Zhang, H. 2021. Counterfactual Zero-Shot and Open-Set Visual Recognition. In *CVPR*, 15404–15414. Computer Vision Foundation / IEEE. 1, 4.3
- Zhang, P.; Li, X.; Hu, X.; Yang, J.; Zhang, L.; Wang, L.; Choi, Y.; and Gao, J. 2021. VinVL: Revisiting Visual Representations in Vision-Language Models. In *CVPR*, 5579–5588. Computer Vision Foundation / IEEE. A.7

Zhao, B.; Fu, Y.; Liang, R.; Wu, J.; Wang, Y.; and Wang, Y. 2019. A Large-Scale Attribute Dataset for Zero-Shot Learning. In *CVPR Workshops*, 398–407. Computer Vision Foundation / IEEE. 1, 2.1, A.1

A Appendix

A.1 Prompt Details

We cluster the attributes to define k class-specific prompt sets for each ZSL dataset (task) as shown in Table 3.

For SUN dataset, (Patterson and Hays 2012) have already divided those scene attributes into four parts: “function”, “material”, “surface_property”, and “spatial_property”. As shown in Table 5, we further split them into 14 prompt sets requiring that the attributes within one set describe different characteristics toward the same aspect of the image. For example, we put “boating” and “driving” from the original “function” part into the more specific prompt set of “transportation function”.

The details of the prompt sets of AWA2 (Xian et al. 2019) are shown in Table 6. The attribute categories of “color”, “pattern”, “shape” and “texture” are from ImageNet (Deng et al. 2009), and part of the categories are from the LAD (Zhao et al. 2019).

While for CUB (Welinder et al. 2010) we simply extract the prefix from the attribute names as the prompt, e.g., we extract the “wing_color” prefix from the attribute “has_wing_color:brown”, and make the “brown” as an attribute belongs to the “wing_color” prompt set. Particularly, different prompt sets may have intersections, e.g., the attribute “spotted” belongs to the prompt sets of “wing_pattern” and “head_pattern” simultaneously. More details are shown in Table 7.

A.2 Details for Experience in Sec. 4

Table 3: Dataset statistics. “# Pro.” and “# Att.” refer to the number of prompt sets and attributes in each dataset. S/U denotes the seen/unseen class.

Dataset	# Pro.	# Att.	# Class	# Images
			Total (S/U)	Training / Testing
CUB	28	312	200 (150 / 50)	7,057 / 4,731
SUN	14	102	717 (645 / 72)	10,320 / 4,020
AWA2	12	85	50 (40 / 10)	23,527 / 13795
AWA2-KG	17	120	50 (40 / 10)	23,527 / 13795

Specifically, we use Swin-base (Liu et al. 2021c) as the vision transformer encoder for SUN, and DeiT-base (Touvron et al. 2021) for CUB, AWA2 and AWA2-KG. Both of their versions are pre-trained on ImageNet-1k. Let $ENC_{vis}(\cdot)$, $ENC_{lan}(\cdot)$, $ENC_{cro}(\cdot)$ be the encoding function of vision transformer, PLM, and cross attention layer respectively. We apply Bert-base (Devlin et al. 2019) as the PLM encoder. We take the output embedding of [CLS] in ENC_{vis} and the whole output hidden state of ENC_{lan} as the input to ENC_{cro} . The cross attention layer number K is set to 1. For each step in T_{CSG} , when applying \mathcal{L}_{acl} , we select $2 c^-$ (i.e., select 2 images from each c^-) and $1 c^+$ for each original image x . For those coefficients, we set λ_{ar} to 0.01, λ_{con} to 0.05, r_{rap} to 0.5, and τ to 0.05 for all datasets. Other dataset-specific hyperparameters are shown in Table 4. We use the AdamW optimizer ($\beta_1 = 0.9$, $\beta_2 = 0.999$), and set the batch size to 50 and the learning rate to $3e-5$. All the experiments are performed on three RTX 3090Ti GPUs. AWA2, which

has the largest scale among our benchmarks which leads to least variance, is selected for all ablation studies.

Table 4: Hyperparameter settings in four datasets.

Dataset	λ_{cmr}	λ_{acl}	γ	ρ
AWA2	1	0.01	0.8	0.4
CUB	5	0.001	0.6	0.4
SUN	1	0.01	0.5	0.5
AWA2-KG	0.5	0.01	0.7	0.4

A.3 Statistics for Attribute

Figure 7 shows part of the statistics about attribute co-occurrence and the imbalanced attribute distribution. Particularly, we define the frequency for those attributes as

$$Freq(a) = \frac{\sum_{c' \in \mathcal{C}} \mathbb{I}[a \in \mathcal{A}^{c'}]}{|\mathcal{C}|} \times 100\%, \quad (17)$$

where $\mathbb{I}[a \in \mathcal{A}^{c'}]$ is 1 if a is in $\mathcal{A}^{c'}$, and 0 otherwise.

In order to measure the degree for attribute co-occurrence, we define the following metric:

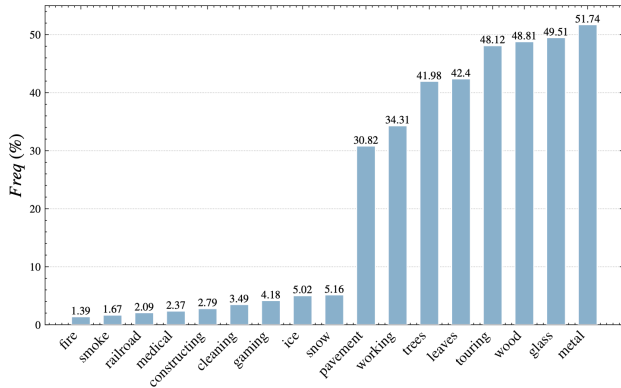
$$R_{co-occ}(a_i \leftarrow a_j) = \frac{\sum_{c' \in \mathcal{C}} \mathbb{I}[a_i \in \mathcal{A}^{c'} \& a_j \in \mathcal{A}^{c'}]}{\sum_{c' \in \mathcal{C}} \mathbb{I}[a_i \notin \mathcal{A}^{c'} \& a_j \in \mathcal{A}^{c'}]}. \quad (18)$$

For example, “flowers” appears with “leaves” 39 times, but “flowers” alone only appears 10 times, then $R_{co-occ}(leaves \leftarrow flowers) = 3.9$, and $Freq(flowers) = 49/717 \times 100\% = 6.83\%$. We observe that the distribution of different attributes varies greatly, and some unforeseen attribute pairs open appear together like (“cloth” \leftarrow “paper”) and (“clouds” \leftarrow “sand”).

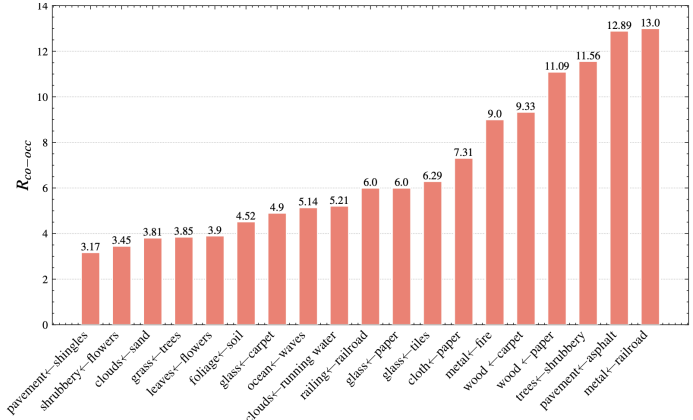
A.4 Semantic Grounding and Visualization

Figure 8 visualizes the dense-attention maps on several test images in SUN. Compared with the BaseModel that only uses ENC_{vis} , our DUET can detect more accurate attribute regions that humans pay attention to. For example, for the “lock chamber” and “tunnel rail outdoor” images, we observe that the BaseModel fails to ground the “railroad” attribute, which is an infrequent attribute with the frequency of 2.09%. Attribute imbalance issue may be the reason that BaseModel wrongly predicts these two images as “landing deck” and “fishpond”.

Moreover, since “waves”, “soil”, “asphalt” and “running water” always occur with “pavement”, “ocean”, “foliage” and “clouds” respectively, the BaseModel would fail to distinguish them in predicting the “flood”, “cavern indoor”, “palace”, and “creek” images which do not contain those latter accompanying attributes. In contrast, DUET better grounds those semantic attributes, leading to better overall performance. Lastly, our model also retains sensitivity for those key characteristics that are not obviously marked out in attribute set such as the teacups in “teashop” and the animals in “ranch”.



(a) Attribute imbalance



(b) Attribute co-occurrence

Figure 7: Statistics about attribute co-occurrence and the imbalanced attribute distribution.

A.5 Sampling Strategy

We employ a heuristic process to let the model select those c^+ whose \mathcal{A}^{c^+} are more *inconsistent*, and c^- whose \mathcal{A}^{c^-} are more *similar*, compared with \mathcal{A}^c . Concretely, we measure the class similarity via the Manhattan distance:

$$\text{Sim}(c, c') = 1/\text{Dist}(c, c'), \quad (19)$$

$$\text{Dist}(c, c') = \sum_{i=1}^A |z_i^c - z_i^{c'}|, \quad (20)$$

and then set the class c' as positive or negative with a probability:

$$P(c^- \leftarrow c' | a_i^c, c) = \frac{\text{Sim}(c, c')^2}{\sum_{\hat{c} \in \mathcal{C}^-} \text{Sim}(c, \hat{c})^2}, \quad (21)$$

$$P(c^+ \leftarrow c' | a_i^c, c) = \frac{\text{Dist}(c, c')^2}{\sum_{\hat{c} \in \mathcal{C}^+} \text{Dist}(c, \hat{c})^2}, \quad (22)$$

where $c' \in \mathcal{C}^+$ and $c' \in \mathcal{C}^-$.

A large number of experiments were conducted and we just selected the most optimal settings (highlight with **bold**):

- Regarding the strategy for choosing the target attributes, we have test (i) the random sampling; (ii) **the linear weighted random sampling** in Eq. (2); (iii) the non-linear weighted random sampling (simple based on squaring or softmax).
- When it comes to the strategy for sampling contrastive classes, we have tested (i) the linear weighted random sampling; (ii) the non-linear weighted random sampling (**based on squaring** in Eq. (21) and (22) or simple softmax).
- When it comes to the metric for class distance, we have tested (i) **the Manhattan distance** in Eq. (20); (ii) the Euclidean distance; (iii) the Cosine similarity.

A.6 Cross-Attention Layer in Sec. 3.2

Each cross-attention layer consists of one bi-directional cross-attention block, two self-attention blocks and two feed-forward blocks. A residual connection and layer normalization are added after each block. Specifically, let $h^k = \{h_1^k, \dots, h_N^k\}$ be the input features of the k -th attention block

$B_k(h^0)$ is the output of Enc , the output state h^{k+1} is computed by

$$\tilde{h}_i^{k+1} = \sum_{m=1}^M W_m^{k+1} \left\{ \sum_{j=1}^N A_{i,j}^m \cdot V_m^{k+1} h_j^k \right\}, \quad (23)$$

$$h_i^{l+1} = \text{LayerNorm} \left(h_i^k + \tilde{h}_i^{k+1} \right), \quad (24)$$

$$A_{i,j}^m \propto \exp \left[(Q_m^{k+1} h_i^k)^T (K_m^{k+1} h_j^k) \right], \quad (25)$$

where $A_{i,j}^m$ denotes the attention weights between elements i and j in the m -th attention head, which is normalized by $\sum_{j=1}^N A_{i,j}^m = 1$. Besides, W_m^{k+1} , query (Q_m^{k+1}), key (K_m^{k+1}) and value (V_m^{k+1}) are learnable weights for m -th head. Remarkably, given any h_i^k, h_j^k is in the set of $\{h_j^k\}$ when B_k is the self-attention block. Contrarily, when B_k is the cross-attention block, $\{h_i^k\}$ and $\{h_j^k\}$ should be originated from different encoders and have no intersection.

A.7 Related Work for PLMs

Stacked by multiple transformer (Vaswani et al. 2017) blocks, the pre-trained language models (PLMs) store an amount of knowledge via learning universal language representations on Internet corpora, which can prevent researchers from training a new model from scratch and benefits downstream NLP tasks. The **Mask Language Model** (MLMs) (2019; 2019; 2021; 2020) are pre-trained by recovering the masked semantic unit in a sentence, which play important roles among all those PLMs. Specifically, the masked semantic unit in BERT (Devlin et al. 2019) is the word token, which is a sequence of characters that are grouped together to express some basic semantic information. Cui et al. (Cui et al. 2021) design a whole word masking (WWM) strategy, where the model always masks all tokens corresponding to a whole word at once. Yin et al. (Yin et al. 2020) propose TaBERT to linearize the tables which makes PLMs understand the structured data.

Inspired by the major success of transformer in NLP field, researchers have recently applied this architecture to CV fields (2021b; 2021; 2021; 2021; 2021; 2021c). For example, the **Vision Transformer** (ViT) (Dosovitskiy et al. 2021) applies the sequences of image patches into pure transformer

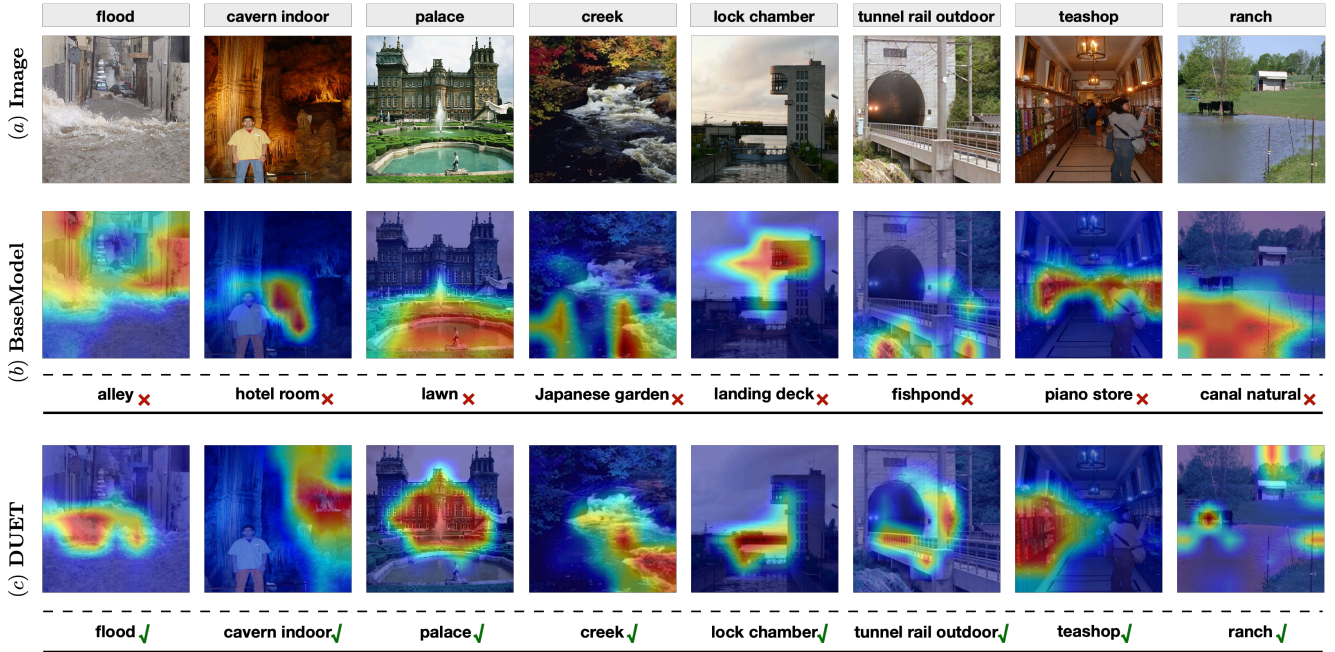


Figure 8: Visualization of attention maps together with attribute grounding results. (a) Original images. (b) BaseModel: Only using ENC_{vis} without cross-modal semantic grounding (CSG) and attribute-level contrastive learning (ACL). (c) DUET.

for image classification. Based on ViT, Touvron et al. (Touvron et al. 2021) further distill the knowledge from CNN-based model, while Swin Transformer (Liu et al. 2021c) computes attention within a local window via partitioning the window into multiple sub-patches.

Previous **Vision-Language Pre-training (VLP)** models (2019; 2019; 2021; 2020) also benefit many multi-modal tasks like visual question answering (VQA) and natural language visual reasoning (NLVR2). But normally, when a multi-modal network is applied to a single-modal task, its performance drops rapidly due to the missing modality. Not to mention performing on a zero-shot single-modal task.

In this paper, we design a novel architecture DUET, which is the first work to extend the PLM architecture to ZSL image classification task under a multi-modal paradigm. Instead of simply taking a fixed semantic embedding as the input (Nawaz, Cavazza, and Bue 2022), our model leverages the knowledge within a large scale PLM via a cross-modal semantic grounding method, as shown in Figure 2(b).

A.8 Vision Encoder Selection

Pre-trained on ImageNet-21k, the Vision Transformer (ViT) (Dosovitskiy et al. 2021) applies the sequences of image patches into a pure transformer for image classification, where a learnable embedding is applied to the sequence of embedding patches whose state serves as the image representation. Based on ViT, DeiT (Touvron et al. 2021) further distills knowledge from a CNN-based model and select a better hyperparameter combination, which trains on only the ImageNet-1k database but achieves comparable performance with ViT. Swin (Liu et al. 2021c) uses a multi-stage hierarchical architecture which computes attention within

a local window via partitioning the window into multiple sub-patches. To capture interactions between different windows, window partitioning in Swin is gradually shifted along the hierarchy of the network to capture overlapping regions, which is suitable for capturing *multi-scale attributes in SUN dataset*. Thus, in this paper, we use Swin-base as the vision transformer encoder for SUN, and DeiT-base¹ for CUB, AWA2, and AWA2-KG, which are all pre-trained on ImageNet-1k with a fixed patch size of 16×16 pixels. Specifically, *for a fair comparison, we utilize the official conversion script² to make the timm-based³ Swin model compatible with the huggingface⁴ transformer library.*

A.9 Attribute prediction in Sec. 4.5

Specifically, we feed an image into the well-trained DUET together with a crafted template:

$$\underbrace{..|color: [MASK]}_{\text{Prompt}} \underbrace{haspart: [MASK]}_{\text{Prompt}}|.., \quad (26)$$

which contains all prompt names \hat{P} with a [MASK] token attached behind each of them. Those mask representations are used for attribute token prediction, where those tokens from the attributes in the prompt set constitute the predictable candidate tokens in PLM’s vocabulary. The token could be mapped into corresponding attributes (maybe

¹huggingface.co/facebook/deit-base-distilled-patch16-224

²github.com/huggingface/transformers/blob/main/src/transformers/models/swin/convert_swin_timm_to_pytorch.py

³github.com/rwightman/pytorch-image-models

⁴huggingface.co/

more than one) for score accumulation. Then we select those attributes whose prediction score rank within the top-3 as the results, and normalize their scores by dividing each of them by their sum. We also normalize those confidence scores from the real-value attribute vectors in the original SUN dataset via global Min-Max normalization, i.e. $z_j^c = 100\% \times (z_j^c - \min(z_i)) / (\max(z_i) - \min(z_i))$. Then we choose those highly confident attributes, and denote them as the ground truth (GT) attributes.

Table 5: Details for the prompts in SUN.

prompt	attributes
transportation function	boating, driving, biking, climbing, swimming, digging
environment function	transporting, sunbathing, touring, hiking, camping, reading, bathing, eating, socializing, congregating, sports, playing, working
technical function	studying, teaching, research, diving, cleaning, queuing, competing, exercise, gaming, audience, farming, constructing, shopping, medical, using tools, business, praying
coarse material	fencing, railing, wire, asphalt, pavement, brick, concrete, metal, paper, wood, linoleum, plastic, stone, ocean
specific material	railroad, flowers, shingles, carpet, tiles, cloth, sand, marble, waves, running water, still water, ice, snow, smoke, fire
natural material	trees, grass, vegetation, shrubbery, foliage, leaves, soil, glass, clouds
light	natural light, direct sun/sunny, indoor light
surface	worn, glossy, matte, sterile, damp, dry, dirty, rusty
temperature	warm, cold
origin property	natural, man made
area	open, semi enclosed, enclosed
horizon	far away horizon, no horizon, rugged scene
direction	vertical, horizontal
feeling	symmetrical, cluttered, scary, soothing, stressful

Table 6: Details for the prompts in AWA2.

prompt	attributes
color	black, white, blue, brown, gray, orange, red, yellow
pattern	patches, spots, stripes
texture	furry, hairless, tough skin
shape	big, small, bulbous, lean
has part	flippers, hands, hooves, pads, paws, long leg, long neck, tail, chew teeth, meat teeth, buck teeth, strain teeth, horns, claws, tusks, smelly, muscle
behaviour	flies, hops, swims, tunnels, walks
character	fast, slow, strong, weak, hibernate, inactive, nocturnal, active, agility
limb	bipedal, quadrupedal
diet	fish, meat, plankton, vegetation, insects
role	forager, grazer, hunter, scavenger, skimmer, stalker, domestic
habitat	new world, old world, arctic, coastal, desert, bush, plains, forest, fields, jungle, mountains, ocean, ground, water, tree, cave
habit	hibernate, fierce, timid, smart, group, solitary, nestspot

Table 7: Details for the prompts in CUB.

prompt	attributes
bill shape	curved, dagger, hooked, needle, hooked seabird, spatulate, all purpose, cone, specialized
wing color	blue, brown, rainbow, purple, auburn, grey, yellow, olive, green, pink, orange, black, white, red, buff
upperparts color	blue, brown, rainbow, purple, auburn, grey, yellow, olive, green, pink, orange, black, white, red, buff
underparts color	blue, brown, rainbow, purple, auburn, grey, yellow, olive, green, pink, orange, black, white, red, buff
breast pattern	solid, spotted, striped, multi colored
back color	blue, brown, rainbow, purple, auburn, grey, yellow, olive, green, pink, orange, black, white, red, buff
tail shape	forked, rounded, notched, fan shaped, pointed, squared
upper tail color	blue, brown, rainbow, purple, auburn, grey, yellow, olive, green, pink, orange, black, white, red, buff
head pattern	spotted, malar, crested, masked, unique, eyebrow, eyering, plain, eyeline, striped, capped
breast color	blue, brown, rainbow, purple, auburn, grey, yellow, olive, green, pink, orange, black, white, red, buff
throat color	blue, brown, rainbow, purple, auburn, grey, yellow, olive, green, pink, orange, black, white, red, buff
eye color	blue, brown, purple, auburn, grey, yellow, olive, green, pink, orange, black, white, red, buff
bill length	same as head, longer than head, shorter than head
forehead color	blue, brown, rainbow, purple, auburn, grey, yellow, olive, green, pink, orange, black, white, red, buff
under tail color	blue, brown, rainbow, purple, auburn, grey, yellow, olive, green, pink, orange, black, white, red, buff
nape color	blue, brown, rainbow, purple, auburn, grey, yellow, olive, green, pink, orange, black, white, red, buff
belly color	blue, brown, rainbow, purple, auburn, grey, yellow, olive, green, pink, orange, black, white, red, buff
wing shape	round, pointed, broad, conical, long
size	large, small, very large, medium, very small
shape	water upright perching, marsh chicken, long leg, duck, owl, gull, hummingbird, pigeon, tree clinging, hawk, sandpiper, upland ground, swallow, perching
back pattern	solid, spotted, striped, multi colored
tail pattern	solid, spotted, striped, multi colored
belly pattern	solid, spotted, striped, multi colored
primary color	blue, brown, rainbow, purple, auburn, grey, yellow, olive, green, pink, orange, black, white, red, buff
leg color	blue, brown, rainbow, purple, auburn, grey, yellow, olive, green, pink, orange, black, white, red, buff
bill color	blue, brown, rainbow, purple, auburn, grey, yellow, olive, green, pink, orange, black, white, red, buff
crown color	blue, brown, rainbow, purple, auburn, grey, yellow, olive, green, pink, orange, black, white, red, buff
wing pattern	solid, spotted, striped, multi colored